View Article Online / Journal Homepage / Table of Contents for this issue
Dynamic Article Links

PCCP

Cite this: *Phys. Chem. Chem. Phys.*, 2012, **14**, 16392–16399

www.rsc.org/pccp

PAPER

Investigation of interstitial hydrogen and related defects in ZnO†

Jörg Koßmann*[a] and Christof Hättig[b]

Received 20th August 2012, Accepted 22nd October 2012
DOI: 10.1039/c2cp42928d

We investigate defects in bulk zinc oxide by performing embedded cluster calculations within the density functional theory using the PBE functional. We obtain and discuss equilibrium structures and vibrational spectra of interstitial hydrogen species and of hydrogen complexes at zinc vacancies and at substitutional atoms like copper, beryllium, manganese and calcium in zinc positions. All of these defects differ in their vibrational frequencies which can be assigned to existing experimental data with an agreement that surpasses the results of earlier calculations within the local (spin) density approximation. This leads to a better understanding of these bulk defects and helps to answer some open questions, as *e.g.* the assignment of a signal observed in infra red spectra at 3326 cm^{-1}. Furthermore, the computed vibrational spectra may serve as a benchmark and assist in the interpretation of future experimental results.

Published on 23 October 2012. Downloaded by Ruhr Universitat Bochum on 1/16/2019 10:24:40 AM.

1 Introduction

Zinc oxide is a widely used material,[1,2] probably best known as zinc white due to its usage as white pigment. It is a semiconductor with a wide band gap[3] of 3.4 eV and is therefore also used in the field of opto-electronics.[4–8]

The investigation of different kinds of defects in ZnO bulk is a hot topic in the current scientific discussion (see ref. 9 for an overview of recent findings). It has been shown that hydrogen can diffuse into the ZnO bulk and form stable subsurface and bulk hydrogen species which can act as shallow donors.[10–15] Vibrational frequencies for such species have been observed in infra red (IR) experiments,[16,17] but the assignment of these frequencies to the structures found in computational studies is controversially discussed in the literature.[18–20]

Another interesting result of recent research is the evidence for a 'hidden' (*i.e.* IR inactive) hydrogen species which could be observed even without any special hydrogen pretreatment in as grown ZnO and which can be converted into the above mentioned well known donor species upon heating.[21] The characterization of these 'hidden' hydrogen species is a major issue in the recent scientific discussion and there are more and more results indicating that this species may be an interstitial molecular hydrogen species.[17,21–24]

There have also been a number of theoretical investigations using the local (spin) density approximation (L(S)DA) to reproduce the vibrational frequencies of interstitial atomic hydrogen species in ZnO bulk.[18–20,25] While some of them fail to reproduce experimental results, others do not discuss all relevant hydrogen species in the ZnO bulk. Furthermore, there are huge differences between the predicted vibrational frequencies of the respective interstitial hydrogen species which make assignments of measured frequencies based on these computational results questionable. To the best of our knowledge, no calculation of vibrational frequencies for all relevant species using a method beyond the local (spin) density approximation has been reported in the literature. Only very recently Du and Biswas calculated the stretch frequencies for some molecular hydrogen species with a hybrid functional.[24] They did, however, not include any corrections for the anharmonicity and for the errors of the density functional.

We hope to enrich the current scientific discussion by presenting our calculated vibrational spectra of relevant hydrogen species and related defects in ZnO bulk, using a method—described in the next section—that has already been proven to give an accurate description of reaction processes on ZnO systems[26] and allows the computation of simulated IR spectra of complex ZnO systems, which are in good agreement with experiment.[27] Our results may serve as a benchmark for the assignment of experimentally obtained vibrational spectra and may add a further point of view (beyond the LDA approximation) in controversially discussed questions concerning hydrogen related defects in ZnO.

2 Computational details

For the description of the bulk defects, we used the embedded cluster approach as described in our previous work.[26,27]

[a] *Atomistic Modelling and Simulation, ICAMS, Ruhr-Universität Bochum, D-44801 Bochum, Germany. E-mail: joerg.kossmann@ruhr-uni-bochum.de*
[b] *Lehrstuhl für Theoretische Chemie, Ruhr-Universität Bochum, D-44801 Bochum, Germany. E-mail: christof.haettig@rub.de*

† Electronic supplementary information (ESI) available: Coordinates of the ideal quantum cluster (without any defects and adatoms), coordinates of ECPs, coordinates of all relaxed atoms of all TZVPP optimized structures discussed in this paper, total electronic energies (TZVPP basis), zero point vibrational energies (SVP basis), unscaled harmonic frequencies, and IR intensities. See DOI: 10.1039/c2cp42928d

 This journal is © the Owner Societies 2012

View Article Online

Published on 23 October 2012. Downloaded by Ruhr Universitat Bochum on 1/16/2019 10:24:40 AM.

All calculations were done with the TURBOMOLE program package.[28,29]

In our model system we assume an ideal wurtzite structure of ZnO with experimental[30–33] lattice parameters $a = 3.2495$ Å, $b = 5.2069$ Å and the internal parameter $u = 0.3825$. Out of this ideal bulk structure a small cluster (quantum cluster), consisting of 162 atoms (without any defects or additional atoms), was cut out of the ZnO bulk and embedded in a three dimensional periodic point charge array using the periodic electrostatic embedded cluster method (PEECM).[34] In order to avoid an artificial attraction of the electrons of the quantum cluster by the nearby positive embedding point charges, we added a 28 e^- effective core potential (ECP)[35] at the 211 cations (Zn^{2+}) in the direct neighborhood of the quantum cluster in order to mimic the repulsion caused by the missing core electrons (the coordinates of the ideal quantum cluster and of surrounding ECPs are provided as ESI†). By adding or removing atoms to or from the quantum cluster we obtained the input structures for the defect species in ZnO. These quantum clusters are described by density functional theory (DFT) with the Perdew–Burke–Ernzerhof (PBE) functional.[36] In ref. 37 it has been shown that this exchange correlation functional gives an accurate description of the ZnO structure.

In first geometry optimizations[38] for these systems we employed a small split valence basis with a single set of polarization functions (SVP),[39] which consists of 3s2p1d contracted basis functions for O and C, 2s1p for H and 5s3p2d for Cu and Zn. Only the coordinates of 101 atoms in the outer shell of the quantum cluster were kept fixed to avoid artifacts from the boundary to the electrostatic embedding. The relaxed structures were used to compute the Hessian matrix and the dipole gradients by numerical differentiation (with a step width of 0.02 a.u. for the Cartesian coordinate displacements) of the energy gradients and dipole moments. In this way, normal modes, harmonic vibrational frequencies, and IR intensities were obtained,[40] as well as the zero point vibrational energies E_{ZPVE}.†

A standard approach to correct for errors due to the harmonic approximation, the approximate exchange correlation functional, and the finite basis set is to scale the raw DFT results for the harmonic frequencies with predetermined empirical correlation factors.[41,42] In ref. 27 we determined such scaling factors for adsorbates on ZnO surfaces and for the surface itself by fitting calculated harmonic vibrational frequencies for a test set of 22 molecules (H_2O, CH_3OH, H_2CO, CH_4, acetone, ethane, ethene, CO, CO_2, HF, LiH, HCOOH, methyl formate, dimethyl ether, acetaldehyde, ethynol, 2-propenal, propane, methylacetate, ZnO_2, ZnH_2, HgH_2) to experimental reference data.[43–46] We obtained for these type of systems with DFT/PBE/SVP an average scaling factor of 1.004, which is also used in the following.

To check for remaining basis set errors in the computed equilibrium structures and to obtain better converged electronic energies and bond lengths, we did subsequently improved geometry optimizations in an accurate triple zeta valence basis set with two sets of polarization functions (TZVPP),[47,48] which consists of 5s3p2d1f contracted basis functions for O/C and for H and Zn/Cu of, respectively, contracted 3s2p1d and 6s4p3d1f functions. For all species discussed in the current paper, the TZVPP optimized structure† differs only slightly from the one obtained in the SVP basis. The root mean square deviation of the bond lengths in SVP and TZVPP optimized structures was less than 0.04 Å for all species discussed in this work.

With the electronic energies E_{TZVPP} obtained with the TZVPP basis and with the zero point vibrational energy E_{ZPVE} one can compute enthalpies H as:

$$H = E_{TZVPP} + E_{ZPVE} + E_{trans} + E_{rot} + pV$$

The translational (E_{trans}), rotational (E_{rot}), and pV terms vanish for bulk species, but are non-zero for molecules in the gas-phase. The latter contributions have been evaluated similar as in ref. 27 for a temperature of 500 K. This gives $E_{trans} + E_{rot} + pV = 0.005542$ a.u. for linear and $E_{trans} + E_{rot} + pV = 0.006334$ a.u. for non-linear free molecules.

3 Results and discussion

3.1 Interstitial hydrogen species

Fig. 1 shows possible positions for an additional hydrogen atom within the wurtzite structure of zinc oxide and the commonly used nomenclature. Such an additional hydrogen atom can be incorporated centered in a ZnO bond orthogonal ($BC_\perp$) or parallel ($BC_\parallel$) to the c-axis or in the corresponding anti-bonding positions ($AB_\perp$ and $AB_\parallel$).

Cutouts of the equilibrium structure are shown in Fig. 2. The related formation enthalpies and wave numbers of the OH stretch vibrations are listed in Table 1. When talking of a formation enthalpy in this context, we mean the reaction enthalpy of the formation of these species out of the ideal wurtzite structure and free H_2:

$$\tfrac{1}{2}H_2(g) + ZnO \rightarrow H(ZnO) \qquad (1)$$

The formation enthalpies for the four species $BC_\perp$, $BC_\parallel$, $AB_\perp$, and $AB_\parallel$ are very similar. The insertion of a hydrogen atom in a BC position is only slightly (in the order of about 10 kJ mol^{-1}) preferred upon the AB position, and the $BC_\parallel$ species is the most stable one. Apparently, this is caused by the slightly stronger OH bonds of both BC species. Also earlier calculation within the local density approximation[10,18,19] have shown that all four variants have quite similar energies and that the BC species are energetically more favoured. While in ref. 10 the $BC_\perp$ species is the most stable one with a 2 kJ mol^{-1} lower

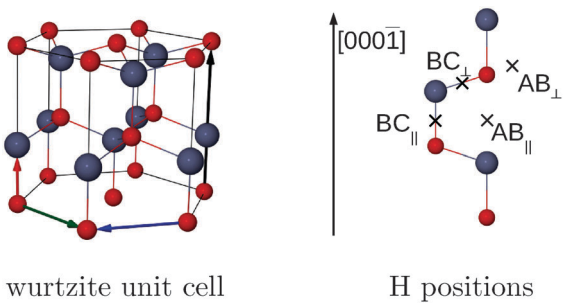


Fig. 1 The wurtzite structure of the ZnO bulk (left) and assumed positions for interstitial hydrogen (right). Zinc atoms: big, blue; oxygen atoms: small, red.

View Article Online

Published on 23 October 2012. Downloaded by Ruhr Universitat Bochum on 1/16/2019 10:24:40 AM.

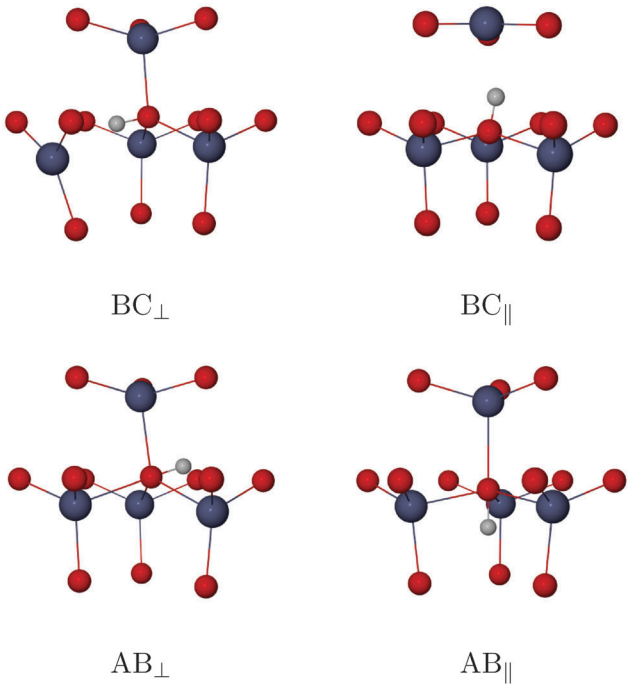


Fig. 2 Cutouts of relaxed structures of interstitial hydrogen defects in ZnO (color code: see Fig. 1, hydrogen atoms: small, white spheres).

Table 1 Frequencies and formation enthalpies of hydrogen in ZnO species. All frequencies are given in cm^{-1} and all enthalpies in kJ mol^{-1}. ΔH_f is the enthalpy of formation w.r.t to free H_2 and the ideal bulk structure (according to eqn (1)). For comparison with calculated O–H stretch frequencies experimentally measured values are shown

	ΔH_f	ν_{calc}(OH)	ν_{exp}(OH)
$BC_\perp$	139	3548	3611[a]
$BC_\parallel$	132	3538	
$AB_\perp$	141	3320	3326[a,b]
$AB_\parallel$	146	3331	
H_{cage}	221	—	—

[a] From ref. 16. [b] From ref. 17.

electronic energy, ref. 18–20 agree that the $H_{BC_\parallel}$ defect has the lowest energy (14 kJ mol^{-1}–20 kJ mol^{-1} lower than the $BC_\perp$ species).

The increased strength of the OH bond of the BC defects is also reflected by the redshifts (up to 228 cm^{-1}) of the OH stretch frequencies of the AB species and also by the slight elongation of the OH bond, which is 0.97 Å for the $BC_\perp$, 0.98 Å for $BC_\parallel$ species and 0.99 Å for both AB structures. This difference between the stretch frequencies of the AB an BC species has also been observed in experimental investigations,[16,49] although the reported splitting is 50 cm^{-1} larger. The stretch frequencies of the AB species are in very good agreement with earlier experimental results which report a wave number of 3326 cm^{-1} [16,17,50,51] assigned to interstitial hydrogen species. In recent IR experiments[52] with high resolution Noei *et al.* could resolve the peak at 3326 cm^{-1} even further into two individual signals at 3337 cm^{-1} and 3313 cm^{-1}. The observed splitting between the bands for the two AB species of 24 cm^{-1} resembles quite well the difference of 10 cm^{-1} between the calculated OH stretch frequencies of the parallel and orthogonal AB species. This nice agreement between theory and experiment corroborates the assignment in Table 1.

In both BC species, the Zn atom of the disturbed bond is strongly displaced from its original position in the ideal bulk structure. Its distance to the oxygen, which is now bound to the inserted hydrogen, increases from 1.99 Å ($BC_\parallel$) and 1.97 Å ($BC_\perp$) to 2.97 Å ($BC_\parallel$) and 2.99 Å ($BC_\perp$), respectively. This larger disturbance of the bulk structure causes a larger error due to the finite cluster size and *probably* explains why the deviation between the measured and the calculated wave numbers for the OH stretch modes is somewhat larger for the BC species (up to 73 cm^{-1}).

Another species, which is energetically unfavoured, is obtained when a H atom is positioned near the center of a Zn_6O_6 'cage' of the wurtzite structure. We will denote this species as H_{cage}, a cutout of the equilibrium structure of this species is shown in Fig. 5. In the relaxed H_{cage} structure, the hydrogen atom is not exactly positioned in the center but slightly shifted along the [000$\bar{1}$] direction, so that the distances to the three Zn atoms at the 'bottom' of this cage are larger (2.64 Å, 2.68 Å, and 2.69 Å) than those to the 'upper' three Zn atoms (1.95 Å, 1.95 Å and 2.10 Å). Hence, this species can be seen as a hydrogen in anti-bonding position referring to the three Zn atoms nearby (distances 2.0 Å–2.1 Å). Nevertheless, the H atom interacts in this position barely with the bulk structure and is in particular not bound to a Zn or O atom which is confirmed by the spin density shown in Fig. 3. Because of the unpaired electron of the neutral hydrogen atom, which is inserted in the ideal bulk structure, all of the systems we have discussed so far are open shell systems. For the two BC and two AB species the unpaired electron is considerably delocalized. This supports the prediction of earlier periodic LDA calculations[10,13] which stated that the electron of the interstitial hydrogen atom is transferred to the conduction band. In contrast to this, the unpaired electron of a hydrogen atom in the 'cage' position is clearly localized. It stays close to the proton and is not transferred to the conduction band. This is supported by the absence of strong ZnH stretch vibrations for the 'cage' species. In fact the hydrogen atom contributes only hindered translation modes to the vibrational spectrum at 640 cm^{-1}, 676 cm^{-1} and 729 cm^{-1}. Furthermore, performing a population analysis based on occupation numbers[53] reveals that the partial charge of the hydrogen atom is +0.12 for the H_{cage}, while it is +0.24 for the BC and +0.29 AB species. This is a further proof for the

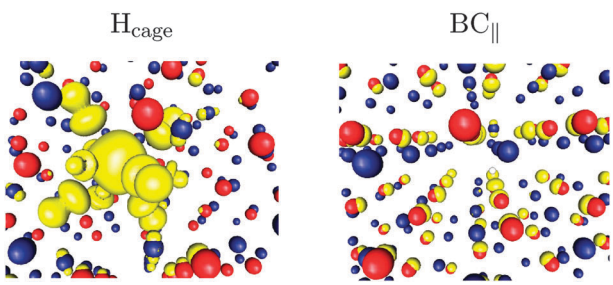


Fig. 3 Iso surface (yellow) for a spin density difference of 0.001 (color code: oxygen atoms red; zinc atoms blue; hydrogen atoms white).

 This journal is © the Owner Societies 2012

View Article Online

Published on 23 October 2012. Downloaded by Ruhr Universitat Bochum on 1/16/2019 10:24:40 AM.

stronger delocalization of the hydrogen's electron if the interstitial hydrogen atom occupies an AB or BC position.

3.2 Interstitial molecular hydrogen species

So far we have discussed the insertion of a single neutral hydrogen atom in the ideal wurtzite structure of ZnO. Now we focus on the investigation of two interstitial hydrogen atoms close to each other into the ZnO bulk to answer the question whether there is a stable molecular hydrogen species in the ZnO bulk that can be identified in experimental measurements by its vibrational spectra.

The cutouts of optimized structures of the most stable species are shown in Fig. 4 and 5. To compare the corresponding enthalpies of formation with those of the single interstitial H atoms discussed in Section 3.1, it is necessary to consider the formation enthalpies per H atom, which is half of the reaction enthalpy for the formation reaction out of free H_2 and defect free ZnO:

$$H_2(g) + ZnO \rightarrow H_2(ZnO) \qquad (2)$$

These enthalpies, denoted as $\frac{1}{2}\Delta H_f$, are listed in Table 2 together with the vibrational frequencies of these species.

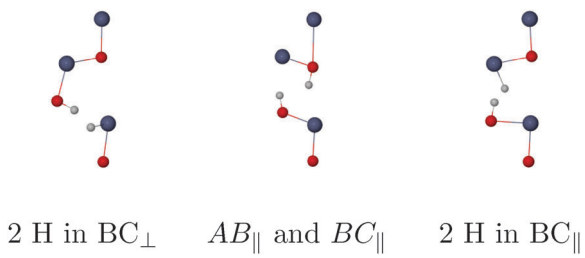


Fig. 4 Cutouts of equilibrium structures of neighboring H and H_2 interstitials in ZnO (color code: see Fig. 2).

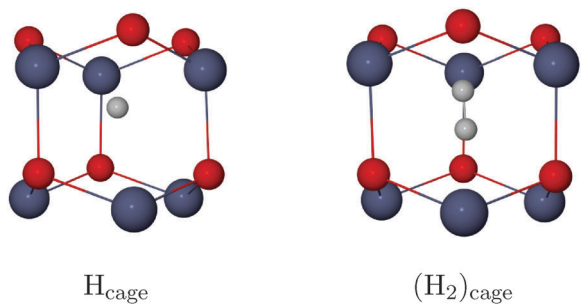


Fig. 5 Cutouts of equilibrium structures of a Hydrogen atom and a H_2 molecule in an interstitial 'cage' position (color code: see Fig. 2).

Table 2 Calculated vibrational frequencies and enthalpies of formation of molecular H_2 and neighboring H species. All wave numbers in cm^{-1}. All enthalpies are formation enthalpies per H atom (according to eqn (2)) and are given in kJ mol^{-1}

	$\frac{1}{2}\Delta H_f$	ν(OH)	ν(ZnH)	ν(HH)
$2H_{cage}$	259	—	—	—
$AB_{\parallel}$ and $BC_{\parallel}$	132	3352, 3480	—	—
2H in $BC_{\parallel}$	106	2472	1458	—
2H in $BC_{\perp}$	99	2875	1570	—
$(H_2)_{cage}$	82	—	—	4151

Two hydrogen atoms in neighboring 'cage' positions do not affect each other strongly. They have the same distances to the nearby Zn atoms as in the case of the previously discussed single H_{cage} species, but the enthalpy per hydrogen atom is slightly larger. Again no strong ZnH stretch modes are present and only vibrations ($\nu(HZn_2)$ and $\delta(HZn_2)$ modes) resulting from hindered translations of the hydrogen atoms with wave numbers below 900 cm^{-1} are predicted by our calculations.

A more favorable configuration for two hydrogens in the bulk is obtained if one H is placed in $AB_{\parallel}$ and the other one in the $BC_{\parallel}$ position. The formation enthalpies are quite similar to those of a single hydrogen atom in an AB or BC position, but the frequencies of the OH stretch modes are slightly shifted due to a weak interaction between the two hydrogen atoms. Hence the H in the $AB_{\parallel}$ position seems to have a stronger bond to the oxygen atom, while the H in the $BC_{\parallel}$ position seems to exhibit a weaker OH-bond.

A geometry optimization starting from a structure with an H_2 molecule inserted in the $BC_{\parallel}$ position leads to another kind of species ($2H_{BC_{\parallel}}$) in which—besides a weaker OH bond with a bond length of 1.02 Å and a strongly redshifted OH stretch frequency—a ZnH bond with a bond length of 1.68 Å is formed. Hence, there is a weak interaction between the two hydrogen atoms, but they are definitely single hydrogen species, which is confirmed by the absence of an HH stretch vibration. A similar species is the analogue structure with two hydrogen atoms inserted in a bond orthogonal to the *c*-axis ($2H_{BC_{\perp}}$). The lengths of the OH (1.00 Å) and the ZnH bond (1.66 Å) are similar as in the $BC_{\parallel}$ variant. The wave number of the OH stretch frequency is 402 cm^{-1} higher, while the ZnH stretch mode has a 112 cm^{-1} higher wave number. Thus, in this configuration both bonds are strengthened. The weak increase in the bond strengths is probably also the reason for the slightly lower formation enthalpies compared to the previously discussed species.

The formation enthalpy per hydrogen atom of a $(H_2)_{cage}$ species (see Fig. 5) is, however, even lower. The HH bond length of the optimized structure is 0.75 Å, just as in the case of a single H_2 molecule in vacuum. The HH stretch mode has a wave number of 4151 cm^{-1}, which is slightly lower than the calculated and scaled wave number of a free hydrogen molecule at 4291 cm^{-1}. Therefore it is reasonable to call this species a molecular hydrogen species in the ZnO bulk.

Actually, the existence of such a molecular hydrogen species in ZnO bulk after H_2 exposure has recently been confirmed in Raman measurements by Lavrov *et al.*,[23] where a HH stretch frequency at 4145 cm^{-1} was observed. This molecular bulk species has the lowest formation enthalpy per hydrogen atom and seems to be even more stable than all single atom species shown in Fig. 2. This is also in good agreement with earlier LSDA calculations[20] where an HH stretch frequency of 4032 cm^{-1} has been calculated. Recently, Du *et al.* have also computed the HH stretch frequency of such a defect using a hybrid functional.[24] They obtained a stretch frequency of 4460 cm^{-1} which is blueshifted by 12 cm^{-1} compared to the calculated wave number for free H_2 reported in ref. 24. Since they did not correct for errors due to anharmonicity and the chosen exchange correlation functional, this result is rather arbitrary which is why the results of ref. 24 does not agree with the other calculations and the measured frequency.

View Article Online

Published on 23 October 2012. Downloaded by Ruhr Universitat Bochum on 1/16/2019 10:24:40 AM.

The formal removal of an O^{2-} anion from the ideal wurtzite structure leads to an $V_O{}^{2+}$ defect. At such a vacancy a meta-stable[24] H_2–$V_O{}^{2+}$ species can be formed. The HH stretch frequencies of this defect is 3991 cm^{-1}. This stronger redshift—compared to the free hydrogen molecule—allows an easy distinction between this meta-stable species and the interstitial $(H_2)_{cage}$ defect. Despite the larger deviation of the calculated HH stretch frequency for this species from the frequency measured in ref. 23, it might be an alternative candidate for the hidden hydrogen species that should be taken into account in future investigations.

3.3 Hydrogen complexes at zinc vacancies

Another important point defect in ZnO are zinc vacancies (V_{Zn}).[54] Some experiments report OH stretch frequencies which are assigned to hydrogen complexes at such vacancies.[49] Therefore, we investigated nH–V_{Zn} complexes with n = 1,2,3,4 and computed the equilibrium structures which are shown in Fig. 6. In order to compare the formation energies of these complexes, we will discuss the reaction enthalpy per hydrogen atom ($\frac{1}{n}\Delta H_r$) for the formation starting from free H_2 and the empty zinc vacancy, according to the following reaction:

$$\frac{n}{2}H_2(g) + V_{Zn} \rightarrow nH - V_{Zn} \qquad (3)$$

The results are listed together with the OH stretch frequencies in Table 3. The energetically most favoured H–V_{Zn} complexes are those, where the additional hydrogen atom is inserted in a bond-centered position, just as in the vacancy free structures (see Section 3.1). But the BC species are strongly stabilized by the vacancy so that the energy difference between the BC and AB variants is about 100 kJ mol^{-1}, which is ten times as large as in the vacancy free bulk. According to our calculation,

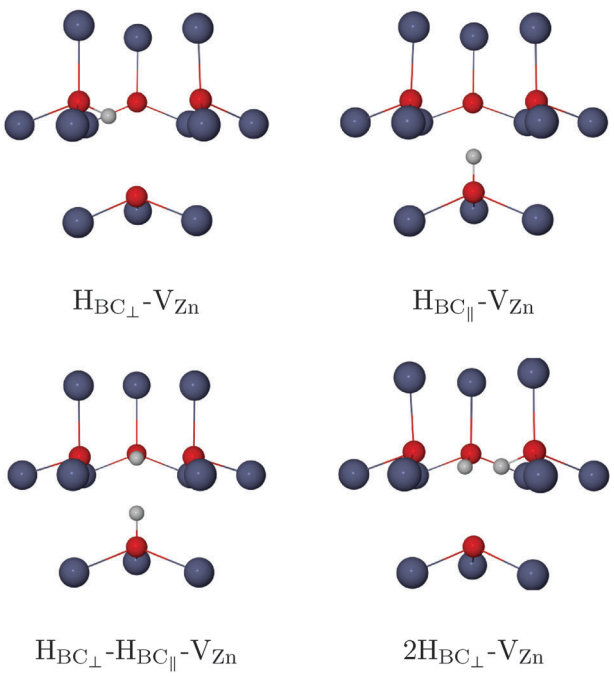


Fig. 6 Cutouts of the equilibrium structures of hydrogen complexes at zinc vacancies (color code: see Fig. 2).

the $H_{AB_\parallel}$–V_{Zn} species, which has the highest formation enthalpy and has also been reported in ref. 20, is a transition state: it has one normal mode with a negative Eigenvalue. In contrast to this, the $AB_\perp$ variant (which has not been reported in ref. 20) has a lower energy and is indeed a local minimum on the potential energy surface.

A comparison of the vibrational spectra for the H–V_{Zn} defects with the interstitial hydrogen species discussed in Section 3.1 reveals that the OH stretch frequencies of the BC species are strongly redshifted by the introduction of the zinc vacancy while the OH bands of the AB variants are blue-shifted. As a result of these shifts, the OH stretch peaks of the AB species now occur at higher frequencies than the corresponding signals of the BC species. Furthermore, the splitting between the signals of the orthogonal and parallel variant is about four times larger than it is for the interstitial hydrogen species without a zinc vacancy.

The LSDA calculations of ref. 20 predicted wave numbers for the BC complexes which are up to 176 cm^{-1} lower than the PBE results presented by us, but the calculated values for the $AB_\parallel$ species are nearly the same at both levels of theory (difference 12 cm^{-1}).

Assuming that a second hydrogen atom prefers a BC position leads to the $2H_{BC_\perp}$–V_{Zn} and the $H_{BC_\parallel}$–$H_{BC_\perp}$–V_{Zn} species which have a nearly identical enthalpy of formation per hydrogen atom (the difference is only 4 kJ mol^{-1}) that is only 20–30 kJ mol^{-1} larger than for the H_{BC}–V_{Zn} defects.

The vibrational spectra of these two 2H–V_{Zn} complexes are characterized by the bands from two normal modes which are positive and negative linear combinations of the two OH stretch modes. Contrary to what has been assumed in ref. 49, it is according to the current results not possible to assign these signals to individual OH bonds of the complex. Compared with the vibrational frequencies observed in ref. 49 the calculated frequencies are slightly higher (25 cm^{-1} and 50 cm^{-1} for species $H_{BC_\parallel}$–$H_{BC_\perp}$–V_{Zn}; 79 cm^{-1} and 74 cm^{-1} for species $2H_{BC_\perp}$–V_{Zn}), which, as mentioned above, can be explained by the constraints for the geometry optimization in a finite cluster model. Also the calculated frequency splitting between the two signals (63 cm^{-1} for species $H_{BC_\parallel}$–$H_{BC_\perp}$–V_{Zn} and 31 cm^{-1} for species $2H_{BC_\perp}$–V_{Zn}) is in good agreement with the splitting of 38 cm^{-1} observed in ref. 49.

The $H_{BC_\parallel}$–$H_{BC_\perp}$–V_{Zn} complex has also been studied in ref. 20 within the LSDA where a frequency splitting of 39 cm^{-1} has been found and the OH stretch frequencies are 84 cm^{-1} and 83 cm^{-1} lower than the experimental observations.

The LSDA calculations agree with our PBE calculations qualitatively regarding the decreasing stability of 3H- and 4H–V_{Zn} complexes. Adding further hydrogen atoms leads to complexes with higher formation enthalpies. Furthermore the OH bond strength of these complexes is lower which leads to strongly redshifted OH stretch frequency—the 4H–V_{Zn} complex even exhibits an OH stretch band below 3000 cm^{-1}.

3.4 Hydrogen complexes as substitutes at the Zn position

ZnO can be doped with copper.[55–58] Such a doping can lead to the formation of Cu–H complexes which have already been observed experimentally.[55,59] We have studied Cu–H complexes

 This journal is © the Owner Societies 2012

View Article Online

Published on 23 October 2012. Downloaded by Ruhr Universitat Bochum on 1/16/2019 10:24:40 AM.

Table 3 OH stretch frequencies in cm^{-1}, OH bond lengths (d(OH)) in Å, and reaction enthalpies per hydrogen atom ($\frac{1}{n}\Delta H_r$, according to eqn (3)) in kJ mol^{-1} of nH–V_{Zn} complexes

Species	$\frac{1}{n}\Delta H_r$	d(OH)	ν(OH)[a]	ν(OH)[b]	ν_{exp}(OH)[c]
$H_{BC_\perp}$–V_{Zn}	−277	0.99	3448	3272	—
$H_{BC_\parallel}$–V_{Zn}	−274	0.99	3393	3255	—
$H_{AB_\parallel}$–V_{Zn}[d]	−163	0.98	3542	3554	—
$H_{AB_\perp}$–V_{Zn}	−178	0.98	3490	—	—
$2H_{BC_\perp}$–V_{Zn}	−254	0.99, 0.99	3391, 3424	—	3312, 3350
$H_{BC_\perp}$–$H_{BC_\parallel}$–V_{Zn}	−250	0.99, 0.99	3337, 3400	3228, 3267	—
$3H_{BC_\perp}$–V_{Zn}	−167	0.99, 0.99, 0.99	3329, 3333, 3379	—	—
$2H_{BC_\perp}$–$H_{BC_\parallel}$–V_{Zn}	−166	0.99, 0.99, 0.99	3191, 3277, 3327	—	—
$4H$–V_{Zn}	−108	0.99, 0.99, 0.99, 1.00	2799, 3010, 3077, 3085	—	—

[a] Calculated in this work. [b] Calculated in ref. 20. [c] Observed in ref. 49. [d] Transition state.

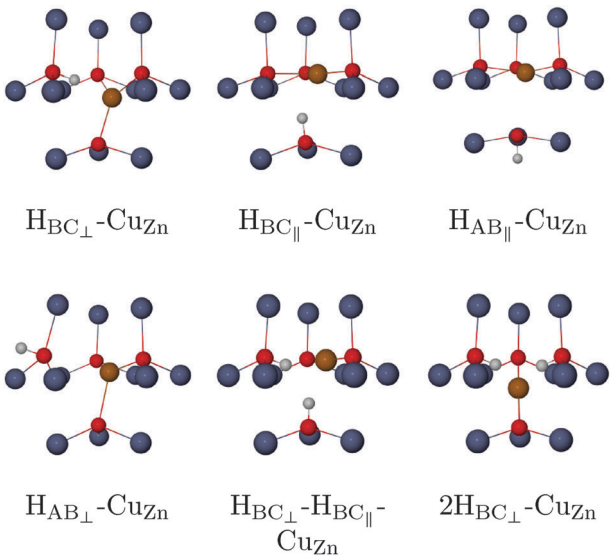


Fig. 7 Cutouts of equilibrium structures of H–Cu_{Zn} and 2H–Cu_{Zn} complexes (color code: see Fig. 2, brown spheres are copper atoms).

at Cu_{Zn} defects which are formed starting from the ideal wurtzite structure by the substitution of a zinc atom by a copper atom (see also ref. 57). Fig. 7 shows the relaxed geometries of these complexes. In Table 4 we compare the OH stretch frequencies and the reaction enthalpy (ΔH_r) of the formation process of the Cu–H complexes out of free hydrogen in the gas phase and the pure Cu_{Zn} defect:

$$\frac{n}{2}H_2(g) + Cu_{Zn} \rightarrow nH - Cu_{Zn} \qquad (4)$$

Also at such a Cu_{Zn} defect, an additional single hydrogen atom prefers again a BC position. The resulting H_{BC}–Cu_{Zn} complexes orthogonal and parallel to the c-axis are, respectively, 49 kJ mol^{-1} and 67 kJ mol^{-1} lower in energy than the corresponding AB variants. The OH stretch frequency of the AB species are, similar as for the H–V_{Zn} complexes, strongly blueshifted by 268 cm^{-1}–370 cm^{-1} compared to the OH bands of the BC defects. Again, the splitting between the variants with the OH bond orthogonal and parallel to the c-axis is quite large (38 cm^{-1} for the AB species and even 69 cm^{-1} for the BC species). Therefore, it should be easier to resolve *e.g.* the individual $BC_\parallel$ and $BC_\perp$ peaks in the experimental spectrum. Compared to the experimental results of ref. 59, where a main peak at 3191.8 cm^{-1} has been reported, the calculated frequencies of the BC species (3192 cm^{-1} and 3123 cm^{-1}) are in good agreement. In fact, the calculated wave number of the $BC_\perp$ species—which has furthermore the lowest enthalpy of formation—is identical with the observed one, but of course this 'perfect agreement' is far beyond the accuracy of the applied method and therefore rather the result of an accidental good error cancellation. Besides this main peak at 3191.8 cm^{-1}, ref. 59 reports 19 side peaks with much lower intensities and wave numbers in the range of about 3180 cm^{-1}–3500 cm^{-1}. These signals may originate from less stable species occurring after Cu and H doping in ZnO and further investigations are needed in order to accurately interpret these side peaks. Nevertheless, it is interesting, that, although the calculated formation enthalpies of both BC species are quite the same, only one main peak has been observed in ref. 59, which suggests that under experimental conditions one BC species is favoured.

We investigated two different 2H–Cu_{Zn} complexes ($H_{BC_\perp}$–$H_{BC_\parallel}$–Cu_{Zn} and $2H_{BC_\perp}$–Cu_{Zn}, see Fig. 7) in which each of the H atoms occupies a BC position. The formation enthalpies per hydrogen atom (−2 kJ mol^{-1} for $H_{BC_\perp}$–$H_{BC_\parallel}$–Cu_{Zn} and 1 kJ mol^{-1} for $2H_{BC_\perp}$–Cu_{Zn}) of these complexes are about 50 kJ mol^{-1} larger than for the H_{BC}–Cu_{Zn} species. Thus 2H–Cu_{Zn} species are energetically less favoured. The calculated

Table 4 Vibrational frequencies and reaction enthalpies of H–X_{Zn} complexes, where X = Zn, Be, Mg, Ca, Cu is a substituent in the Zn position. ΔH_r is the reaction enthalpy according to eqn (5) in kJ mol^{-1}, all wave numbers are given in cm^{-1}

	None (Zn)		Be		Mg		Ca		Cu	
Substituent X_{Zn} =	ν(OH)	ΔH_r	ν(OH)	ΔH_r	ν(OH)	ΔH_r	ν(OH)	ΔH_r	ν(OH)	ΔH_r
$H_{AB_\parallel}$	3331	146	$\rightarrow BC_\parallel$		3284	152	3479	119	3493	18
$H_{AB_\perp}$	3320	141	3426	135	3413	137	3453	92	3455	−5
$H_{BC_\parallel}$	3538	132	3486	102	3452	164	$\rightarrow AB_\perp$		3123	−49
$H_{BC_\perp}$	3548	139	3627	111	$\rightarrow AB_\perp$		$\rightarrow AB_\perp$		3192	−54

View Article Online

Published on 23 October 2012. Downloaded by Ruhr Universitat Bochum on 1/16/2019 10:24:40 AM.

OH stretch frequencies of the complexes (3261 cm^{-1} and 3284 cm^{-1} for $H_{BC_\perp}$–$H_{BC_\parallel}$–Cu_{Zn}; 3233 cm^{-1} and 3264 cm^{-1} for $2H_{BC_\perp}$–Cu_{Zn}) are about 90 cm^{-1}–110 cm^{-1} higher than those observed in ref. 55 (3347 cm^{-1} and 3374 cm^{-1}), but the computed splitting between the modes which can be interpreted as symmetric and antisymmetric linear combinations of the two individual OH stretch modes is with, respectively, 32 cm^{-1} and 23 cm^{-1} in excellent agreement with the measurements reported in ref. 55, where a splitting of 27 cm^{-1} has been found.

For comparison, we also investigated similar H–Be_{Zn}, H–Mg_{Zn}, and H–Ca_{Zn} defects. In these complexes, a zinc cation of the ideal wurtzite structure is not replaced by a copper atom, but by a group II (earth alkali) atom. Table 4 summarizes the calculated vibrational frequencies and a comparison of the enthalpies for the following reactions:

$$\tfrac{1}{2}H_2(g) + X_{Zn} \rightarrow H\text{–}X_{Zn} \qquad (5)$$

Especially the H–Ca_{Zn} are of interest. In ref. 19 it has been suggested that such a defect might be a possible alternative origin for the IR signal at 3326 cm^{-1}, which we assign to the $H_{AB_\parallel}$ and $H_{AB_\perp}$ species.

Again, the local minima of the potential energy surface are quite flat, which is why the geometry optimizations easily converge towards the global minimum which is of course much deeper in energy. Hence, in some cases we could not identify some of the possible flat local minima and therefore only focus at the most stable structures.

If the zinc atom is replaced by a Be atom, the interstitial hydrogen atom again prefers the BC positions, similar as for the H–Cu_{Zn} and H–V_{Zn} species. But the substitution with a Mg or Ca cation, which both have large ionic radii, leads to a destabilization of the BC positions, so that the $AB_\perp$ position becomes favoured. With the exception of $H_{AB_\parallel}$–Mg—which is not the preferred H–Mg complex—all H–X species with X = Be, Mg, Ca have OH stretch frequencies above 3410 cm^{-1}. Therefore our calculations do not support the assumption in ref. 19.

4 Conclusions

Our PBE calculations† mostly support the qualitative results of several previous L(S)DA calculations,[18–20,25] but show a better and more consistent agreement with experimental results.[16,17,52] Atomic hydrogen can occupy interstitial positions in ZnO. The resulting $H_{BC_\perp}$, $H_{BC_\parallel}$, $H_{AB_\perp}$, and $H_{AB_\parallel}$ species have similar formation enthalpies, but can be distinguished by their vibrational spectra. We obtained vibrational spectra for interstitial hydrogen species in ZnO bulk which are in good agreement with the experimental findings. They especially support the assignment of the 3326 cm^{-1} signal to interstitial hydrogen atoms in AB positions. Since our calculations further predict OH stretch frequencies of the most stable H–Be_{Zn}, H–Mg_{Zn}, and H–Ca_{Zn} complexes to appear above 3400 cm^{-1}, these types of defects can be excluded as the origin of the peak at 3326 cm^{-1}.

In addition to these atomic interstitial species, we studied also a molecular hydrogen species. We could demonstrate that the molecular interstitial hydrogen species $(H_2)_{cage}$ is a promising candidate to explain the unknown hidden hydrogen species discussed in ref. 21. The computed HH stretch frequency agrees well with the Raman measurements reported in ref. 23.

Hydrogen atoms may also accumulate at zinc vacancies and at Cu_{Zn} defects, where preferentially H–V_{Zn}, 2H–V_{Zn}, H–Cu_{Zn}, and 2H–Cu_{Zn} are formed. These defects have characteristic vibrational spectra which allows us to distinguish such defects from other interstitial hydrogen species. The vibrational spectra obtained for these complexes are in good agreement with experiment.[49,55,59]

For all investigated V_{Zn}, Be_{Zn}, Mg_{Zn}, Ca_{Zn}, and Cu_{Zn} complexes we could show that these defects—which are just a few examples of the large zoo of possible point defects in ZnO—have a strong influence on the stability and on the OH stretch frequencies of nearby interstitial hydrogen species. Hence for the interpretation of experimental spectra it is crucial to consider the amount of such defects.

Acknowledgements

The present work was supported by the Deutsche Forschungsgemeinschaft (DFG) within the framework of the Collaborative Research Center 558 "Metal–Substrate Interactions in Heterogeneous Catalysis" (SFB 558). We acknowledge the fruitful cooperation with Dr Yuemin Wang and Dr Heshmat Noei.

References

1 U. Özgür, Y. Alivov, C. Liu, A. Teke, M. Reshchikov, S. Dogğan, V. Avrutin, S.-J. Cho and H. Morkoç, *J. Appl. Phys.*, 2005, **98**, 041301.
2 C. Klingshirn, *Phys. Status Solidi B*, 2007, **244**, 3027–3073.
3 O. Madelung, M. Schulz and H. Weiss, *Numerical data and functional relationships in science and technology*, Springer-Verlag, Berlin, 1982, vol. 17.
4 J. Zhang, W. Lu and L. Thang, *Phys. Lett. A*, 2002, **299**, 276–281.
5 A. Janotti and C. Van de Walle, *Rep. Prog. Phys.*, 2009, **72**, 126401.
6 Y. Zhu, H. Zhang, X. Sun, S. Feng, J. Xu, Q. Zhao, B. Xiang, R. Wang and D. Yua, *Appl. Phys. Lett.*, 2003, **83**, 144–146.
7 B. Ryu, P. Uthirakumar, J. H. Kang, B. Kwon, S. Chandramohan, H. Kim, H. Kim, J. Ryu, H. Kim and C.-H. Hong, *J. Appl. Phys.*, 2011, **109**, 093116.
8 W. Beek, M. Wienk and R. Janssen, *Adv. Funct. Mater.*, 2006, **16**, 1112–1116.
9 M. McCluskey and J. Jokela, *J. Appl. Phys.*, 2009, **106**, 071101.
10 C. van de Walle, *Phys. Rev. Lett.*, 2000, **85**, 1012–1015.
11 D. Thomas and J. Lander, *J. Chem. Phys.*, 1956, **25**, 1136–1142.
12 K. Ip, M. Overberg, Y. Heo, D. Norton, S. Pearton, C. Stutz, B. Luo, F. R. D. Look and J. Zavada, *Appl. Phys. Lett.*, 2003, **82**, 385–387.
13 H. Qiu, B. Meyer, Y. Wang and C. Wöll, *Phys. Rev. Lett.*, 2008, **101**, 236401.
14 H. Noei, H. Qiu, Y. Wang, M. Muhler and C. Wöll, *ChemPhysChem*, 2010, **11**, 3604–3607.
15 F. Traeger, M. Kauer, C. Wöll, D. Rogalla and H. Becker, *Phys. Rev. B: Condens. Matter Mater. Phys.*, 2011, **84**, 075462.
16 G. Shi, M. Stavola, S. Pearton, M. Thieme, E. Lavrov and J. Weber, *Phys. Rev. B: Condens. Matter Mater. Phys.*, 2005, **72**, 195211.
17 M. McCluskey, S. Jokela and W. Oo, *Physica B*, 2006, **376–377**, 690–693.
18 S. Limpijumnong and S. Zhang, *Appl. Phys. Lett.*, 2005, **86**, 151910.
19 X.-B. Li, S. Limpijumnong, W. Tian, H.-B. Sun and S. Zhang, *Phys. Rev. B: Condens. Matter Mater. Phys.*, 2008, **78**, 113203.
20 M. Wardle, J. Goss and P. Briddon, *Phys. Rev. B: Condens. Matter Mater. Phys.*, 2005, **72**, 155108.

 This journal is © the Owner Societies 2012

View Article Online

21 G. Shi, M. Saboktakin, M. Stavola and S. Pearton, *Appl. Phys. Lett.*, 2004, **85**, 5601–5603.
22 A. Janotti and C. Van de Walle, *Nat. Mater.*, 2007, **6**, 44–47.
23 E. Lavrov, F. Herklotz and J. Weber, *Phys. Rev. Lett.*, 2009, **102**, 185502.
24 M.-H. Du and K. Biswas, *Phys. Rev. Lett.*, 2011, **106**, 115502.
25 J. Bang, E.-A. Choi and K. Chang, *J. Appl. Phys.*, 2009, **106**, 053522.
26 G. Roßmüller, V. Kleinschmidt, J. Koßmann and C. Hättig, *J. Phys. Chem. C*, 2009, **113**, 1418–1425.
27 J. Koßmann, G. Roßmüller and C. Hättig, *J. Chem. Phys.*, 2012, **136**, 034706.
28 R. Ahlrichs, M. Bär, M. Häser, H. Horn and C. Kölmel, *Chem. Phys. Lett.*, 1989, **162**, 165–169.
29 *TURBOMOLE V6.2 2010, a development of University of Karlsruhe and Forschungszentrum Karlsruhe GmbH*, TURBOMOLE GmbH, 1989–2007, since 2007, available from www.turbomole.com
30 R. Wyckoff, *Crystal Structures*, Interscience Publisher, New York, 1965, vol. I.
31 R. Blachnik, J. Chu, R. R. Galazka, J. Geurts, J. Gutowski, B. Hönerlage, D. Hofmann, J. Kossut, R. Lévy, P. Michler, U. Neukirch, T. Story, D. Strauch and A. Waag, *Landolt-Börnstein, New Series III*, Springer-Verlag, Berlin, 1999, vol. 41B.
32 S. Abrahams and J. Bernstein, *Acta Crystallogr.*, 1969, **B25**, 1233–1236.
33 T. Sabine and S. Hogg, *Acta Crystallogr.*, 1969, **B25**, 2254–2256.
34 A. M. Burow, M. Sierka, J. Döbler and J. Sauer, *J. Chem. Phys.*, 2009, **130**, 174710.
35 F. Schautz, H.-J. Flad and M. Dolg, *Theor. Chem. Acc.*, 1998, **99**, 231–240.
36 J. Perdew, K. Burke and M. Ernzerhof, *Phys. Rev. Lett.*, 1996, **77**, 3865–3868.
37 B. Meyer and D. Marx, *Phys. Rev. B: Condens. Matter Mater. Phys.*, 2003, **67**, 035403.
38 M. v. Arnim and R. Ahlrichs, *J. Chem. Phys.*, 1999, **111**, 9183.
39 A. Schäfer, H. Horn and R. Ahlrichs, *J. Chem. Phys.*, 1992, **97**, 2571–2577.
40 J. Neugebauer, M. Reiher, C. Kind and B. Hess, *J. Comput. Chem.*, 2002, **23**, 895–910.
41 J. Merrick, D. Moran and L. Radom, *J. Phys. Chem.*, 2007, **111**, 11683.
42 M. Laury, S. Boesch, O. Haken, P. Sinha, R. Wheeler and A. Wilson, *J. Comput. Chem.*, 2011, **32**, 2339–2347.
43 T. Shimanouchi, in *Tables of Molecular Vibrational Frequencies Consolidated Volume I*, National Bureau of Standards, Washington, DC, USA, 1972, pp. 1–160.
44 W. Person, *Vibrational intensities in infrared and Raman spectroscopy*, Elsevier, Amsterdam, 1982.
45 R. Hochstrasser and J. Wirz, *Angew. Chem.*, 1989, **101**, 183–185.
46 M. Jacox, *J. Phys. Chem. Ref. Data*, 1998, **27**, 115–393.
47 A. Schäfer, C. Huber and R. Ahlrichs, *J. Chem. Phys.*, 1994, **100**, 5829–5835.
48 F. Weigend, M. Häser, H. Patzelt and R. Ahlrichs, *Chem. Phys. Lett.*, 1998, **294**, 143–152.
49 E. Lavrov, J. Weber, F. Börnert, C. Van De Walle and R. Helbig, *Phys. Rev. B: Condens. Matter Mater. Phys.*, 2002, **66**, 165205.
50 S. Jokela and M. McCluskey, *Phys. Rev. B: Condens. Matter Mater. Phys.*, 2005, **72**, 113201.
51 M. McCluskey, S. Jokela, K. Zhuravlev, P. Simpson and K. Lynn, *Appl. Phys. Lett.*, 2002, **81**, 3807–3809.
52 H. Noei and Y. Wang, private communication.
53 C. Erhardt and R. Ahlrichs, *Theor. Chim. Acta*, 1985, **63**, 231–245.
54 A. Kohan, G. Ceder, D. Morgan and C. Van de Walle, *Phys. Rev. B: Condens. Matter Mater. Phys.*, 2000, **61**, 15019–15027.
55 E. Lavrov, J. Weber and F. Börnert, *Phys. Rev. B: Condens. Matter Mater. Phys.*, 2008, **77**, 155209.
56 F. Herklotz, E. Lavrov and J. Weber, *Physica B*, 2009, **404**, 4807–4809.
57 H. Qiu, F. Gallino, C. Di Valentin and Y. Wang, *Phys. Rev. Lett.*, 2011, **106**, 066401.
58 D. Buchholz, R. Chang, J.-Y. Song and J. Ketterson, *Appl. Phys. Lett.*, 2005, **87**, 082504.
59 F. Gärtner and E. Mollwo, *Phys. Status Solidi B*, 1978, **89**, 381–388.

Published on 23 October 2012. Downloaded by Ruhr Universitat Bochum on 1/16/2019 10:24:40 AM.